

# Notes on diffusion networks

–Supplemental Material for “On learning optimized reaction diffusion processes for effective image restoration”–

Yunjin Chen<sup>1,2</sup>

<sup>1</sup>Graz University of Technology    <sup>2</sup>National University of Defense Technology

chenyunjin.nudt@hotmail.com

## Abstract

*This is the supplemental material for our CVPR2015 paper entitled “On learning optimized reaction diffusion processes for effective image restoration”. In this supplemental material, we give detailed derivations of gradients required in training for corresponding diffusion networks. In addition, we also present more image denoising and JPEG deblocking examples.*

## 1. Preliminaries

When we modify the original diffusion equation

$$u_t = u_{t-1} - \left( \sum_{i=1}^{N_k} K_i^t \phi_i^t(K_i^t u_{t-1}) + \lambda^t(u_{t-1} - f_n) \right), \quad (1)$$

to the following version

$$u_t = u_{t-1} - \left( \sum_{i=1}^{N_k} \bar{k}_i^t * \phi_i^t(k_i^t * u_{t-1}) + \lambda^t(u_{t-1} - f_n) \right), \quad (2)$$

we find it introduces some imperfections at the image boundary. The basic reason lies in the fact that, in the case of symmetric boundary condition used in our work,  $K^\top v$  can be interpreted as the convolution with the kernel  $\bar{k}^1$  only in the central region of image  $v$ . This interpretation does not hold for the image boundary. However, in the diffusion equation (2), the convolution kernel  $\bar{k}_i$  is applied to the whole image, thus bringing some artifacts at the boundary. The benefit to use the diffusion equation (2), rather than (1) is that the revised model is more tractable in practice, especially for training, as everything can be done by the convolution operation efficiently.

In order to remove this artifacts, we pad the input image  $u_{t-1}$  for stage  $t$ , as well as the noisy image  $f_n$ , with mirror reflections of itself. This operation is formulated by the sparse “padding” matrix  $P$ . After a diffusion step, we only crop the central region of the output image  $u_t$  for usage. This operation is formulated by the sparse “cropping” matrix  $T$ . When we apply the matrix  $P_T = P \times T$  to an image  $u$ ,  $P_T u$  corresponds to two operations: it first crops the central region of  $u$ , then pads it with mirror reflections.

After taking into account the operation of boundary handling, the exact diffusion process is illustrate in Figure 1. There we have  $u_{tp} = P_T u_t$ .

**In our derivations, we use the symmetric boundary condition for the convolution operation  $k * u$  (image  $u \in \mathbb{R}^{m \times n}$ ,  $k \in \mathbb{R}^{r \times r}$ ). As we know, it is equivalent to the matrix-vector product formulation  $Ku$ , where  $K \in \mathbb{R}^{N \times N}$  is a highly sparse matrix and  $u$  is a column vector  $u \in \mathbb{R}^N$  with  $N = m \times n$ . The result  $k * u$  can also be interpreted with  $Uk$ , where matrix  $U \in \mathbb{R}^{N \times R}$  is constructed from image  $u$  and  $k$  is a column vector  $k \in \mathbb{R}^R$  with  $R = r \times r$ . This formulation is very helpful for the computation of the gradients of the loss function w.r.t. the kernel  $k$ , as  $U^\top v$  ( $v \in \mathbb{R}^N$  is a column vector) can be explicitly interpreted as a convolution operation, which is widely used in classic convolutional neural networks [1]. In the following derivations, we will make use of this equivalence frequently, i.e.,**

$$k * u \iff Ku \iff Uk.$$

<sup>1</sup>Recall that kernel  $\bar{k}$  is obtained by rotating  $k$  180 degrees.

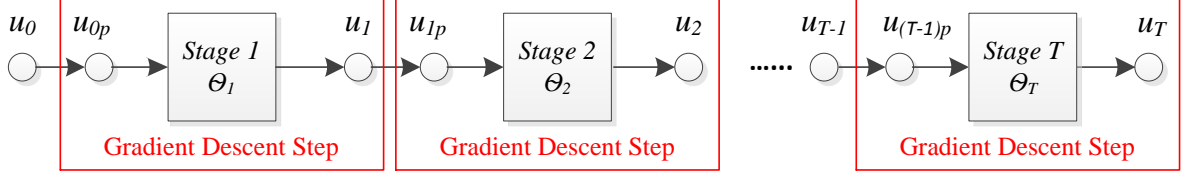


Figure 1. Proposed nonlinear diffusion process with careful boundary handling operation. Note that  $u_{tp} = P_T u_t$ .

The derivations also require matrix calculus. We use the **denominator layout notation**<sup>2</sup> for all the derivations.

## 2. Derivations of learning problem

Given  $S$  training samples  $\{f_n^{(s)}, u_{gt}^{(s)}\}_{s=1}^S$ , where  $f_n^{(s)}$  is the noisy input and  $u_{gt}^{(s)}$  is the corresponding ground truth clean image. Let assume the original image size is  $m \times n$ . We first pad the noisy image  $f_n$  with  $\omega$  pixels, then the resulting image has size  $O = (m + 2\omega) \times (n + 2\omega)$ . We have the corresponding matrix  $T \in \mathbb{R}^{N \times O}$ ,  $P \in \mathbb{R}^{O \times N}$ ,  $P_T \in \mathbb{R}^{O \times O}$  and  $f_{np} \in \mathbb{R}^O$ ,  $u_{gt} \in \mathbb{R}^N$ .

### 2.1. Greedy training

In the greedy training for stage  $t$ , we are to minimize the following loss function w.r.t the model parameters  $\Theta_t = \{\lambda^t, \phi_i^t, k_i^t\}$  of stage  $t$ ,

$$L(\Theta_t) = \sum_{s=1}^S \ell(u_t^{(s)}, u_{gt}^{(s)}) = \sum_{s=1}^S \frac{1}{2} \|T u_t^{(s)} - u_{gt}^{(s)}\|_2^2, \quad (3)$$

where

$$u_t^s = u_{(t-1)p}^s - \left( \sum_{i=1}^{N_k} \bar{k}_i^t * \phi_i^t(k_i^t * u_{(t-1)p}^s) + \lambda^t(u_{(t-1)p}^s - f_{np}^s) \right). \quad (4)$$

Note that in the training for stage  $t$ , the images  $u_{(t-1)p}$  are fixed, served as the input of this feed-forward step.

As the gradient of overall loss function on the whole training datasets can be decomposed to the sum over training samples, in the following derivation, we only consider the case of one training sample for the sake of brevity. The basic result of the gradient of the loss function w.r.t the training parameters  $\Theta_t = \{\lambda^t, \phi_i^t, k_i^t\}$  is given

$$\frac{\partial \ell(u_t, u_{gt})}{\partial \Theta_t} = \frac{\partial u_t}{\partial \Theta_t} \cdot \frac{\partial \ell(u_t, u_{gt})}{\partial u_t}, \quad (5)$$

where  $\frac{\partial \ell(u_t, u_{gt})}{\partial u_t}$  is simply given as

$$\frac{\partial \ell(u_t, u_{gt})}{\partial u_t} = T^\top (T u_t - u_{gt}).$$

Let us define a column vector  $e \in \mathbb{R}^O$  as

$$e = T^\top (T u_t - u_{gt}).$$

Therefore, the main issue is to calculate  $\frac{\partial u_t}{\partial \Theta_t}$  from (4).

**Weight parameter  $\lambda^t$ :** It is easy to see that

$$\frac{\partial u_t}{\partial \lambda^t} = (u_{(t-1)p} - f_{np})^\top. \quad (6)$$

Thus  $\frac{\partial \ell}{\partial \lambda^t}$  is given as

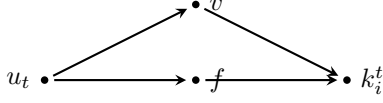
$$\frac{\partial \ell}{\partial \lambda^t} = (u_{(t-1)p} - f_{np})^\top e. \quad (7)$$

<sup>2</sup> [http://en.wikipedia.org/wiki/Matrix\\_calculus](http://en.wikipedia.org/wiki/Matrix_calculus)

**Filters  $k_i^t$ :** Concerning the dependency of  $u_t$  on parameters  $k_i^t$ , it is easy to see the following relationship

$$u_t^s \rightarrow \underbrace{-\bar{k}_i^t}_f * \underbrace{\phi_i^t(k_i^t * u_{(t-1)p})}_v,$$

where  $f$  and  $v$  are two auxiliary variables defined as  $f = -\bar{k}_i^t$  and  $v = \phi_i^t(k_i^t * u_{(t-1)p})$ . Therefore, we get the following dependency relationship,



According to the chain rule, we have

$$\frac{\partial u_t}{\partial k_i^t} = \frac{\partial f}{\partial k_i^t} \cdot \frac{\partial u_t}{\partial f} + \frac{\partial v}{\partial k_i^t} \cdot \frac{\partial u_t}{\partial v}. \quad (8)$$

Note that  $f = -\bar{k}_i^t$ , which can be formulated as  $f = -P_{inv}k_i^t$  with matrix  $P_{inv}$  inverting the kernel vector  $k_i^t$ . Recall the equivalence

$$f * v \iff Fv \iff Vf.$$

Therefore, the first term of (8) is given as

$$\frac{\partial f}{\partial k_i^t} \cdot \frac{\partial u_t}{\partial f} = -P_{inv}^\top V^\top.$$

For the second term, we introduce an additional auxiliary variable  $z$ , defined as  $z = k_i^t * u_{(t-1)p}$ . Then we have  $v = \phi_i^t(z)$ . Recall that

$$z = k_i^t * u_{(t-1)p} \iff U_{(t-1)p} k_i^t.$$

Therefore, we obtain

$$\frac{\partial v}{\partial k_i^t} \cdot \frac{\partial u_t}{\partial v} = \frac{\partial z}{\partial k_i^t} \cdot \frac{\partial v}{\partial z} \cdot \frac{\partial u_t}{\partial v} = U_{(t-1)p}^\top \Lambda F^\top,$$

where  $\Lambda$  is a diagonal matrix  $\Lambda = \text{diag}(\phi_i^{t'}(z_1), \dots, \phi_i^{t'}(z_p))$  ( $\phi_i^{t'}$  is the first order derivative of function  $\phi_i^t$ ). Note that  $F = -\bar{K}_i^t$ . In summary,  $\frac{\partial u_t}{\partial k_i^t}$  is given as

$$\frac{\partial u_t}{\partial k_i^t} = - \left( P_{inv}^\top V^\top + U_{(t-1)p}^\top \Lambda \bar{K}_i^{t\top} \right). \quad (9)$$

Finally, we arrive at the desired gradients

$$\boxed{\frac{\partial \ell}{\partial k_i^t} = - \left( P_{inv}^\top V^\top + U_{(t-1)p}^\top \Lambda \bar{K}_i^{t\top} \right) e}. \quad (10)$$

In practice, we do not need to explicitly construct the matrices  $V, U, \bar{K}_i^t$ . Recall that the product of matrices  $V^\top, U_{(t-1)p}^\top$  and a vector can be computed by the convolution operator [1]. As shown in a previous work [4],  $\bar{K}_i^{t\top}$  can also be computed by the convolution operation with the kernel  $\bar{k}_i^t$  with careful boundary handling. Matrix  $P_{inv}^\top$  is merely a linear operation which inverts the vectorized kernel  $k$ . In the case of a square kernel  $k$ , it is equivalent to the Matlab command

$$P_{inv}^\top k \iff \text{rot90}(\text{rot90}(k)).$$

If we have a closer look at the diffusion equation (4), we find that it has a scaling problem w.r.t the filters  $k_i^t$ . First we know the function  $\phi_i^t$  is free to tune in the training. In this case, if we scale the filter  $k_i^t$  by a factor of  $h$  to generate a new filter  $\hat{k}_i^t = h k_i^t$ , and the corresponding new function  $\hat{\phi}_i^t$  is selected such that  $\hat{\phi}_i^t(hz) = \frac{1}{h} \phi_i^t(z)$ , then we will see that the term  $\bar{k}_i^t * \phi_i^t(k_i^t * u_{(t-1)p})$  keep unchanged, i.e., two different set of parameters  $\{k_i^t, \phi_i^t\}$  and  $\{\hat{k}_i^t, \hat{\phi}_i^t\}$  own exactly the same loss function  $\ell(u_t, u_{gt})$ . In order to get rid of this ambiguity, it is necessary to fix the scale of the filters. In practice, we learn filters with fixed unit norm. Motivated by the finding in [4] that meaningful filters should be zero-mean, we also construct the

training filter  $k$  from the DCT basis  $\mathcal{B} \in \mathbb{R}^{R \times (R-1)}$  (without the DC-component). Therefore, we define each filter  $k \in \mathbb{R}^R$  with

$$k = \mathcal{B} \frac{c}{\|c\|_2}, \quad (11)$$

where  $c \in \mathbb{R}^{R-1}$ . Now the training parameters become  $c$ , and we need to calculate  $\frac{\partial \ell}{\partial c}$ . As shown in (10), we already have  $\frac{\partial \ell}{\partial k}$ , according to the chain rule, we have

$$\frac{\partial \ell}{\partial c} = \frac{\partial k}{\partial c} \cdot \frac{\partial \ell}{\partial k},$$

where  $\frac{\partial k}{\partial c}$  is computed from (11). Let us define an auxiliary variable  $v = \frac{c}{\|c\|_2}$ , we have

$$\frac{\partial k}{\partial c} = \frac{\partial v}{\partial c} \cdot \frac{\partial k}{\partial v} \quad (12a)$$

$$= \frac{\partial v}{\partial c} \cdot \mathcal{B}^\top \quad (12b)$$

$$= \left( \frac{\mathbf{I}}{\|c\|_2} + \frac{\partial[(c^\top c)^{-\frac{1}{2}}]}{\partial c} \cdot c^\top \right) \cdot \mathcal{B}^\top \quad (12c)$$

$$= \left( \frac{\mathbf{I}}{\|c\|_2} + \frac{\partial[(c^\top c)]}{\partial c} \cdot \left(-\frac{1}{2} \frac{1}{\|c\|_2^3}\right) \cdot c^\top \right) \cdot \mathcal{B}^\top \quad (12d)$$

$$= \left( \frac{\mathbf{I}}{\|c\|_2} + 2c \cdot \left(-\frac{1}{2} \frac{1}{\|c\|_2^3}\right) \cdot c^\top \right) \cdot \mathcal{B}^\top \quad (12e)$$

$$= \frac{1}{\|c\|_2} \left( \mathbf{I} - \frac{c}{\|c\|_2} \cdot \frac{c^\top}{\|c\|_2} \right) \cdot \mathcal{B}^\top, \quad (12f)$$

where  $\mathbf{I} \in \mathbb{R}^{(R-1) \times (R-1)}$  is the identity matrix. Combining the Equation (10) and (21), we can obtain the desired gradients of the loss function w.r.t the training parameter  $c_i^t$ , given as

$$\frac{\partial \ell}{\partial c_i^t} = -\frac{1}{\|c_i^t\|_2} \left( \mathbf{I} - \frac{c_i^t}{\|c_i^t\|_2} \cdot \frac{c_i^{t\top}}{\|c_i^t\|_2} \right) \cdot \mathcal{B}^\top \cdot \left( P_{inv}^\top V^\top + U_{(t-1)p}^\top \Lambda \bar{K}_i^{t\top} \right) e \quad (13)$$

**Influence functions  $\phi$ :** According to diffusion equation (4), the dependency of  $u_t$  on the influence function  $\phi_i^t$  is given as

$$u_t \rightarrow -\bar{K}_i^t \cdot \phi_i^t (K_i^t \cdot u_{(t-1)p}). \quad (14)$$

Let us define an auxiliary variable  $y \in \mathbb{R}^O$  as

$$y = K_i^t \cdot u_{(t-1)p}. \quad (15)$$

In our work, function  $\phi_i^t$  is represented as

$$\phi_i^t(z) = \sum_{j=1}^M w_{ij}^t \varphi \left( \frac{|z - \mu_j|}{\gamma} \right), \quad (16)$$

Therefore, the column vector  $\phi_i^t(y) \in \mathbb{R}^O$  can be reformulated via a matrix equation

$$\phi_i^t(y) = G(y) \cdot w_i^t,$$

where  $w_i^t \in \mathbb{R}^M$  is the vectorized version of parameters  $w_{ij}^t$ , matrix  $G(y) \in \mathbb{R}^{O \times M}$  is given as

$$\underbrace{\begin{bmatrix} \varphi\left(\frac{|y_1 - \mu_1|}{\gamma}\right) & \varphi\left(\frac{|y_1 - \mu_2|}{\gamma}\right) & \dots & \varphi\left(\frac{|y_1 - \mu_M|}{\gamma}\right) \\ \varphi\left(\frac{|y_2 - \mu_1|}{\gamma}\right) & \varphi\left(\frac{|y_2 - \mu_2|}{\gamma}\right) & \dots & \varphi\left(\frac{|y_2 - \mu_M|}{\gamma}\right) \\ \vdots & \vdots & \ddots & \vdots \\ \varphi\left(\frac{|y_O - \mu_1|}{\gamma}\right) & \varphi\left(\frac{|y_O - \mu_2|}{\gamma}\right) & \dots & \varphi\left(\frac{|y_O - \mu_M|}{\gamma}\right) \end{bmatrix}}_{G(y)} \underbrace{\begin{bmatrix} w_{i1} \\ w_{i2} \\ \vdots \\ w_{iM} \end{bmatrix}}_{w_i} = \underbrace{\begin{bmatrix} \phi_i(y_1) \\ \phi_i(y_2) \\ \vdots \\ \phi_i(y_Q) \end{bmatrix}}_{\phi_i(y)}. \quad (17)$$

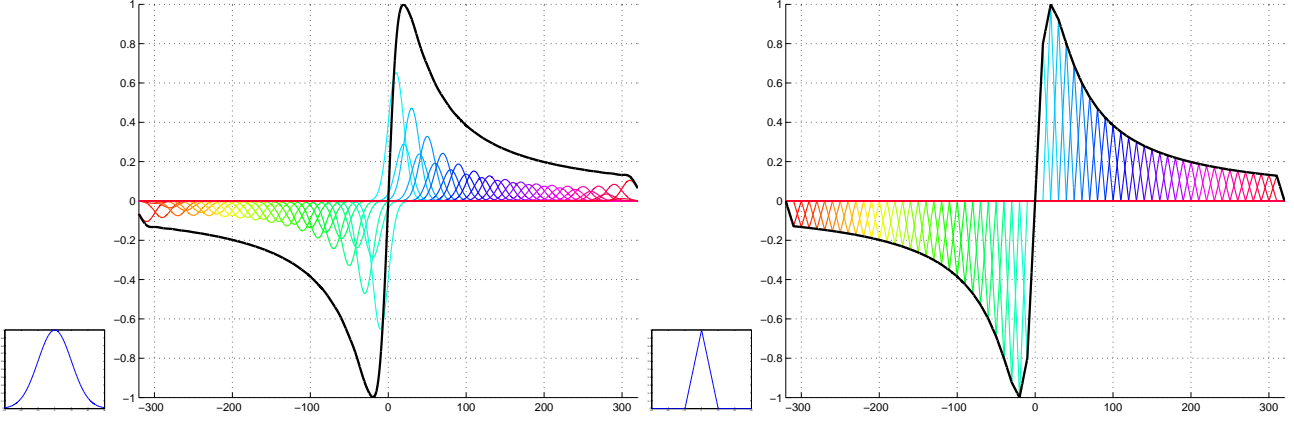


Figure 2. Function approximation via Gaussian  $\varphi_g(z)$  or triangular-shaped  $\varphi_t(z)$  radial basis function, respectively.

Now, it is straightforward to obtain  $\frac{\partial u_t}{\partial w_i^t}$ , given as

$$\frac{\partial u_t}{\partial w_i^t} = -G^\top \bar{K}_i^t{}^\top. \quad (18)$$

Then we can obtain the desired gradients of the loss function w.r.t the parameters of the influence function, written as

$$\frac{\partial \ell}{\partial w_i^t} = -G^\top \bar{K}_i^t{}^\top e. \quad (19)$$

In this paper, we investigate two typical RBFs [8]: (1) Gaussian radial basis  $\varphi_g$  and (2) triangular-shaped radial basis  $\varphi_t$ , which are given as

$$\varphi_g(z) = \varphi\left(\frac{|z - \mu|}{\gamma}\right) = \exp\left(-\frac{(z - \mu)^2}{2\gamma^2}\right)$$

and

$$\varphi_t(z) = \varphi\left(\frac{|z - \mu|}{\gamma}\right) = \begin{cases} 1 - \frac{|z - \mu|}{\gamma} & |z - \mu| \leq \gamma \\ 0 & |z - \mu| > \gamma \end{cases}$$

respectively. The basis functions are shown in Figure 2, together with an example of the function approximation by using two different RBF methods.

In Figure 2, we can see that in the case of triangular-shaped RBF based function approximation any input variable  $z$  only involves two basis functions, *i.e.*, each row of the  $G$  matrix (17) only has two non-zero numbers. **Therefore, we can explicitly make use of this property in the implementation to speed up the computation of Equation (19), *i.e.*, the triangular-shaped RBF based training process is generally faster than the Gaussian RBF based one.**

In the training, the first order derivative of the influence function  $\phi$  is also required as in Equation (13). In the case of Gaussian RBF, the first order derivative is given as

$$\phi'_i(z) = -\gamma \sum_{j=1}^M w_{ij} \exp\left(-\frac{\gamma}{2}(z - \mu_j)^2\right) \cdot (z - \mu_j).$$

In the case of triangular-shaped RBF,  $\phi'$  is defined by a piece-wise constant function as  $\phi$  is a piece-wise linear function. Although the influence function  $\phi$  and its derivative  $\phi'$  is not smooth, the training still works quite well.

In practice, in order to speed up the computation of the function value  $\phi(z)$  and its derivative  $\phi'(z)$  for the case of Gaussian RBF, we approximate these functions with piece-wise linear functions (the function values at discrete points are precomputed and stored in a lookup-table), then the function values at point  $z$  can be retrieved efficiently using linear interpolation.

Concerning the function approximation accuracy, in general, the Gaussian RBF can provide a better approximation for generally smooth function than the triangular-shaped RBF with the same number of basis functions, as the latter generates a piece-wise linear function for approximation. In order to improve the approximation accuracy of the triangular-shaped RBF based method, usually we need to exploit more basis functions relative to the Gaussian RBF based method. However, using

more basis functions will bring an undesired problem of over-fitting. Therefore, certain regularization technique is required. Unfortunately, up to now we have not figured out the best choice for the regularization term.

In our work, we have investigated both function approximation methods, and we find that they generate similar results. We only present the results obtained by the Gaussian RBF due to space limitation. We do not provide a comprehensive comparison of two methods, as it is out of the scope of this paper.

## 2.2. Joint training

In the joint training, the parameters of all stages  $T$  are optimized simultaneously. The joint training task is formulated as

$$\mathcal{L}(\Theta_{1,\dots,T}) = \sum_{s=1}^S \ell(u_T^{(s)}, u_{gt}^{(s)}), \quad (20)$$

where the loss function only depends on  $u_T$ , the output of the final stage  $T$ . The gradients of the loss function w.r.t  $\Theta_t$  is given as

$$\frac{\partial \ell(u_T, u_{gt})}{\partial \Theta_t} = \frac{\partial u_t}{\partial \Theta_t} \cdot \frac{\partial \ell(u_T, u_{gt})}{\partial u_t},$$

where  $\frac{\partial u_t}{\partial \Theta_t}$  has been already done in the preceding subsection. Now the main issue is to calculate  $\frac{\partial \ell(u_T, u_{gt})}{\partial u_t}$ . As we only know

$$e = \frac{\partial \ell(u_T, u_{gt})}{\partial u_T} = T^\top (T u_T - u_{gt}),$$

the standard back-propagation technique widely used in neural networks learning [10] can be used to calculate the desired gradients, which is written as

$$\frac{\partial \ell(u_T, u_{gt})}{\partial u_t} = \frac{\partial u_{t+1}}{\partial u_t} \cdot \frac{\partial \ell(u_T, u_{gt})}{\partial u_{t+1}} \quad (21a)$$

$$= \frac{\partial u_{t+1}}{\partial u_t} \cdot \frac{\partial u_{t+2}}{\partial u_{t+1}} \cdot \frac{\partial \ell(u_T, u_{gt})}{\partial u_{t+2}} \quad (21b)$$

$$= \frac{\partial u_{t+1}}{\partial u_t} \cdot \frac{\partial u_{t+2}}{\partial u_{t+1}} \cdots \frac{\partial u_T}{\partial u_{T-1}} \cdot e. \quad (21c)$$

In practice, (21) is computed using a backward manner starting from the last stage. Now the only thing we need to calculate is  $\frac{\partial u_{t+1}}{\partial u_t}$ . Recall the diffusion process shown in Figure 1, it is straightforward to see that

$$\frac{\partial u_{t+1}}{\partial u_t} = \frac{\partial u_{tp}}{\partial u_t} \cdot \frac{\partial u_{t+1}}{\partial u_{tp}},$$

where  $\frac{\partial u_{tp}}{\partial u_t} = P_T^\top$  according to the equation  $u_{tp} = P_T u_t$ , and  $\frac{\partial u_{t+1}}{\partial u_{tp}}$  can be obtained from the diffusion equation (4).

$$\frac{\partial u_{t+1}}{\partial u_{tp}} = (1 - \lambda^{t+1})\mathbf{I} - \sum_{i=1}^{N_k} K_i^{t+1\top} \cdot \Lambda_i \cdot (\bar{K}_i^{t+1})^\top,$$

where  $\Lambda_i$  is a diagonal matrix  $\Lambda_i = \text{diag}(\phi_i^{t+1'}(z_1), \dots, \phi_i^{t+1'}(z_p))$  with  $z = k_i^{t+1} * u_{tp}$ . Therefore, the overall  $\frac{\partial u_{t+1}}{\partial u_t}$  is given as

$$\frac{\partial u_{t+1}}{\partial u_t} = P_T^\top \cdot \left( (1 - \lambda^{t+1})\mathbf{I} - \sum_{i=1}^{N_k} K_i^{t+1\top} \cdot \Lambda_i \cdot (\bar{K}_i^{t+1})^\top \right).$$

Then the gradients of  $\frac{\partial \ell(u_T, u_{gt})}{\partial u_t}$  can be computed using the backward recurrence described above. Once we have obtained the results of  $\frac{\partial \ell(u_T, u_{gt})}{\partial u_t}$ , it is straightforward to calculate  $\frac{\partial \ell(u_T, u_{gt})}{\partial \Theta_t}$  using the derivations in previous subsection.

## 3. Training for JPEG deblocking

As mentioned in the main paper, in this paper, we consider the JPEG deblocking problem by defining a new variational model, which incorporates the FoE image prior model and the quantization constraint set (QCS).

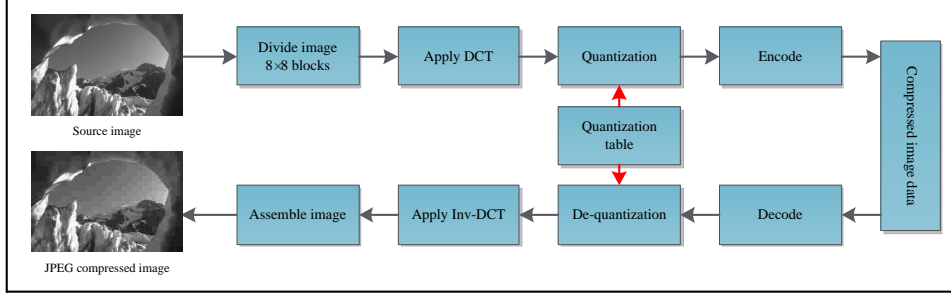


Figure 3. Schematic overview of the JPEG compression and decompression procedure

### 3.1. JPEG compression and the QCS

Figure 3 illustrates all the steps of the JPEG compression and decompression procedure. In the step of quantization, the transformed DCT coefficients of each  $8 \times 8$  block are point-wise divided by the quantization matrix, and then the values are rounded to integer, which is where the loss of data takes place, as the rounding operation is a mapping of “ $\infty \rightarrow 1$ ”. Given an integer number  $d$ , any number in the interval  $[d - \frac{1}{2}, d + \frac{1}{2}]$  is a possible candidate for the original number which is rounded to  $d$ .

With the compressed image data, we only know the integer coefficient data  $(d_{i,j}^I)_{1 \leq i,j \leq 8}$ , where  $I$  indicates a  $8 \times 8$  block indexed by  $I$ , and the quantization matrix  $(Q_{i,j})_{1 \leq i,j \leq 8}$ . Therefore, the possible original DCT coefficients, which yield  $(d_{i,j}^I)$  during the quantization and rounding procedure are given by the interval

$$S_{i,j}^I = [Q_{i,j}(d_{i,j}^I - \frac{1}{2}), Q_{i,j}(d_{i,j}^I + \frac{1}{2})].$$

This result is for the block  $I$ . For the full size image, we just need to repeat this result for each distinct block. All the intervals  $S_{i,j}^I$  associated with each  $8 \times 8$  block form the so-called QCS, which is simply a box constraint determining all possible source images.

### 3.2. Variational model for image deblocking

In our training, an image  $u$  of size  $m \times n$  is padded with  $\omega$  pixels (we set  $\omega = 8$  for this problem). In order to simplify the notation, the interval  $S$  is represented by two column vectors  $a \in \mathbb{R}^O$  and  $b \in \mathbb{R}^O$  ( $O = (m + 2\omega) \times (n + 2\omega)$ ), which correspond to the lower and upper bounds of the intervals  $S_{i,j}^I$ , respectively. We further define a highly sparse matrix  $D \in \mathbb{R}^{O \times O}$ , which makes  $Du$  equivalent to the block-wise DCT transform applied to the two-dimensional image  $u$ .

Given the compressed image data, the QCS is given as the box constraint  $S = [a, b]$ , and the set of possible source image of the compression process is defined as

$$U = \{u \in \mathbb{R}^O \mid (Du)_p \in [a_p, b_p]\}.$$

Then we can define our variational model based on the FoE image prior model and QCS, which reads as

$$\arg \min_{u \in U} E(u) = \sum_{i=1}^{N_k} \rho_i(k_i * u). \quad (22)$$

This is a constrained optimization problem, and it can be rewritten as

$$\arg \min_u E(u) = \sum_{i=1}^{N_k} \rho_i(k_i * u) + \mathcal{I}_S(Du), \quad (23)$$

where

$$\mathcal{I}_S(Du) = \begin{cases} 0 & \text{if } Du \in S, \\ \infty & \text{else.} \end{cases}$$

In this formulation, we exploit the convex set  $S$  instead of set  $U$ , as  $S$  is a box constraint, which is simpler than  $U$ .

As the minimization problem (23) contains the non-smooth indicator function, the standard gradient descent algorithm is not applicable. Therefore, we resort to the more general proximal gradient method [11], which is applicable to solve a class of the following minimization problems

$$\min_u h(u) = f(u) + g(u), \quad (24)$$

where  $f$  is a smooth function and  $g$  is convex (possibly non-smooth) function. The proximal gradient method is defined as

$$u_t = (\mathbf{I} + \tau \partial g)^{-1}(u_{t-1} - \tau \nabla f(u_{t-1})),$$

where  $\tau$  is the step size parameter,  $(\mathbf{I} + \tau \partial g)^{-1}$  denotes the proximal mapping operator. Casting the problem (23) in the form of (24), we have  $f(u) = \sum_{i=1}^{N_k} \rho_i(k_i * u)$  and  $g(u) = \mathcal{I}_S(Du)$ . It is easy to check that

$$\nabla f(u) = \sum_{i=1}^{N_k} \bar{k}_i * \phi_i(k_i * u),$$

with  $\phi_i(z) = \rho'_i(z)$ . We again make the modification  $\bar{k}_i$  to the rigorous formulation  $K_i^\top$ . The proximal mapping with respect to  $g$  is given as the following minimization problem

$$(I + \tau \partial g)^{-1}(\hat{u}) = \arg \min_u \frac{\|u - \hat{u}\|_2^2}{2} + \tau \mathcal{I}_S(Du). \quad (25)$$

As DCT is a orthogonal transform, i.e.,  $D^\top D = DD^\top = \mathbf{I}$ , then we have

$$\|Du - D\hat{u}\|_2^2 = (u - \hat{u})^\top D^\top D(u - \hat{u}) = (u - \hat{u})^\top (u - \hat{u}) = \|u - \hat{u}\|_2^2.$$

For problem (25), let

$$c = Du, \quad \hat{c} = D\hat{u}.$$

Note that the connection between  $c$  and  $u$  (also  $\hat{c}$  and  $\hat{u}$ ) is a mapping of one-to-one.

It turns out that

$$\arg \min_u \frac{\|u - \hat{u}\|_2^2}{2} + \tau \mathcal{I}_S(Du) \iff \arg \min_c \frac{\|c - \hat{c}\|_2^2}{2} + \tau \mathcal{I}_S(c).$$

Obviously, the solution for the minimization problem of right side is given as the following point-wise projection onto the interval, i.e., QCS

$$\tilde{c}_p = \begin{cases} \hat{c}_p & \text{if } \hat{c}_p \in S_p = [a_p, b_p] \\ b_p & \text{if } \hat{c}_p > b_p \\ a_p & \text{if } \hat{c}_p < a_p. \end{cases} \quad (26)$$

Finally, the the solution of  $u$  is given as  $\tilde{u} = D^\top \tilde{c}$ . Therefore, the overall gradient descent step is given as

$$u_t = D^\top \text{proj}_{\text{QCS}} \left( D \left( u_{t-1} - \sum_{i=1}^{N_k} \bar{k}_i * \phi_i(k_i * u_{t-1}) \right) \right), \quad (27)$$

where  $\text{proj}_{\text{QCS}}(\cdot)$  denotes the orthogonal projection onto QCS (26). In our training model, as we consider different filters and influence functions for each stage  $t$ , the accurate diffusion process is given as

$$u_t = D^\top \text{proj}_{\text{QCS}} \left( D \left( u_{t-1} - \sum_{i=1}^{N_k} \bar{k}_i^t * \phi_i^t(k_i^t * u_{t-1}) \right) \right). \quad (28)$$

The projection operator can be represented by the function  $\eta(z)$  show in Figure 4. Therefore, the corresponding gradient descent step (28) can be rewritten as the following formulas by introducing the auxiliary variables  $v$ ,  $z$ , and  $y$ .

$$\begin{cases} u_t = D^\top v \\ v = \eta(z) \\ z = Dy \\ y = u_{t-1} - \sum_{i=1}^{N_k} \bar{k}_i^t * \phi_i^t(k_i^t * u_{t-1}). \end{cases} \quad (29)$$



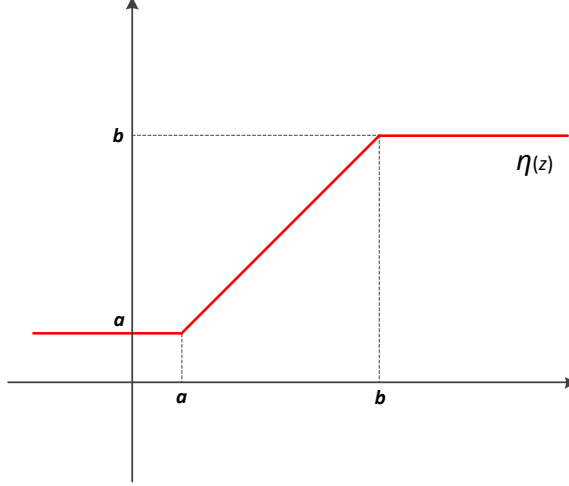


Figure 4. The projection function  $\eta(z)$ .

For the training of this new problem, the training parameters  $\Theta_t$  is given by  $\Theta_t = \{\phi_i^t, k_i^t\}$ . According to the result of (5), for this new training problem, we can make use of the framework presented in the last section and we just need to recalculate  $\frac{\partial u_t}{\partial \Theta_t}$  from (29), which is given as

$$\begin{aligned} \frac{\partial u_t}{\partial \Theta_t} &= \frac{\partial y}{\partial \Theta_t} \cdot \frac{\partial z}{\partial y} \cdot \frac{\partial v}{\partial z} \cdot \frac{\partial u_t}{\partial v} \\ &= \frac{\partial y}{\partial \Theta_t} \cdot D^\top \cdot \text{diag}(\eta'(z)) \cdot D, \end{aligned} \quad (30)$$

where  $\eta'(z) = (\eta'(z_1), \eta'(z_2), \dots, \eta'(z_O))^\top \in \mathbb{R}^O$  with  $\eta'(z_p)$  defined as

$$\eta'(z_p) = \begin{cases} 1 & \text{if } z_p \in [a_p, b_p], \\ 0 & \text{else} \end{cases} \quad (31)$$

Even though we do not consider any smoothing technique for the non-smooth function  $\eta$ , in practice we find that it is not a problem for the training procedure by using the above discontinuous derivative. According to the derivations (9) and (18) in the last section, it is straightforward to calculate  $\frac{\partial y}{\partial \Theta_t}$ , which leads to exactly the same results.

Concerning the joint training model, we can still make use of the same framework presented in the last section and we just need to additionally compute  $\frac{\partial u_t}{\partial u_{t-1}}$ . Taking into account the operation of boundary handling,  $\frac{\partial u_t}{\partial u_{t-1}}$  is given as

$$\begin{aligned} \frac{\partial u_t}{\partial u_{t-1}} &= P_T^\top \cdot \frac{\partial y}{\partial u_{t-1}} \cdot \frac{\partial z}{\partial y} \cdot \frac{\partial v}{\partial z} \cdot \frac{\partial u_t}{\partial v} \\ &= P_T^\top \cdot \left( \mathbf{I} - \sum_{i=1}^{N_k} K_i^t \cdot \Lambda_i \cdot \bar{K}_i^t \right) \cdot D^\top \cdot \text{diag}(\eta'(z)) \cdot D \end{aligned} \quad (32)$$

Combining the derivation results of (30), (32) and the framework presented in the last section, we can reach the formulas required for the training of the JPEG deblocking problem.

#### 4. Denoising and deblocking examples

In this section, we provide examples to illustrate the performance of our trained nonlinear diffusion processes for Gaussian denoising and JPEG deblocking. See Figure 5 and Figure 6 for image denoising examples for noise level  $\sigma = 25$  on the images from the test dataset. Note the differences in the highlighted regions.

We also present the corresponding runtime either on CPU or GPU. We do not count the memory transfer time between CPU/GPU for both GPU implementations (if counted, the run time will nearly double). Note the speed gap between CSF<sub>7×7</sub><sup>5</sup>

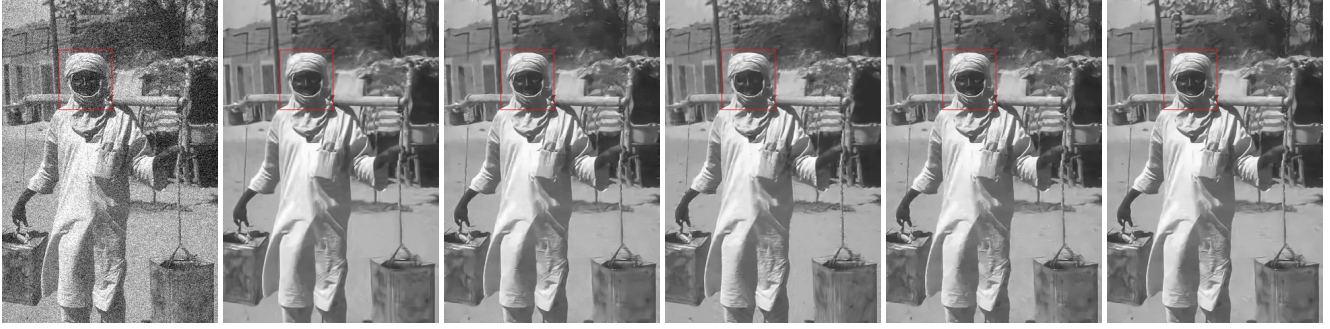
and our model is not mainly caused by the different Matlab/CUDA implementations, but the lower computational expense of our approach.

Figure 7 presents a denoising example on a megapixel-size natural image of size  $1050 \times 1680$ . Overall, nonlocal methods (BM3D and WNNM) are prone to generating artifacts. The  $\text{TRD}_{7 \times 7}^5$  model provides the highest PSNR value, and better preserves tiny image structures, such as the tree branches shown in the highlighted region. Furthermore, our method exhibits the best runtime.

Figure 8 presents four JPEG deblocking examples for the compression quality  $q = 10$ . Note the effectiveness of our trained TRD model, meanwhile, remember that our approach is extremely fast on GPUs.

## References

- [1] J. Bouvrie. Notes on convolutional neural networks. 2006. 1, 3
- [2] K. Bredies and M. Holler. Artifact-free jpeg decompression with total generalized variation. In *VISAPP (I)*, pages 12–21, 2012. 13
- [3] H. Chang, M. K. Ng, and T. Zeng. Reducing artifact in JPEG decompression via a learned dictionary. *IEEE TSP*, 62(3):718–728, 2014. 13
- [4] Y. Chen, R. Ranftl, and T. Pock. Insights into analysis operator learning: From patch-based sparse models to higher order MRFs. *IEEE TIP*, 23(3):1060–1072, 2014. 3
- [5] K. Dabov, A. Foi, V. Katkovnik, and K. O. Egiazarian. Image denoising by sparse 3-d transform-domain collaborative filtering. *IEEE TIP*, 16(8):2080–2095, 2007. 11, 12
- [6] A. Foi, V. Katkovnik, and K. Egiazarian. Pointwise shape-adaptive DCT for high-quality denoising and deblocking of grayscale and color images. *IEEE TIP*, 16(5):1395–1411, 2007. 13
- [7] S. Gu, L. Zhang, W. Zuo, and X. Feng. Weighted nuclear norm minimization with application to image denoising. In *CVPR*, 2014. 11, 12
- [8] Y. H. Hu and J.-N. Hwang. *Handbook of neural network signal processing*. CRC press, 2010. 5
- [9] J. Jancsary, S. Nowozin, and C. Rother. Loss-specific training of non-parametric image restoration models: A new state of the art. In *ECCV*, pages 112–125, 2012. 13
- [10] Y. LeCun, L. Bottou, Y. Bengio, and P. Haffner. Gradient-based learning applied to document recognition. *Proceedings of the IEEE*, 86(11):2278–2324, 1998. 6
- [11] Y. Nesterov and I. E. Nesterov. *Introductory lectures on convex optimization: A basic course*, volume 87. Springer, 2004. 8
- [12] U. Schmidt and S. Roth. Shrinkage fields for effective image restoration. In *CVPR*, 2014. 11, 12



(a) Noisy, 20.17dB (b) BM3D, 28.60dB (c) CSF<sub>7×7</sub><sup>5</sup>, 28.83dB (d) WNNM, 28.82dB (e) TRD<sub>5×5</sub><sup>5</sup>, 28.85dB (f) TRD<sub>7×7</sub><sup>5</sup>, **28.97dB**



(g) Noisy, 20.17dB



(h) BM3D, 36.78dB/CPU: 2.5s



(i) CSF<sub>7×7</sub><sup>5</sup>, 37.15dB/GPU: 0.55s



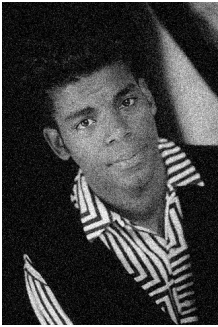
(j) WNNM, 36.95dB/CPU: 393.2s



(k) TRD<sub>5×5</sub><sup>5</sup>, 37.04dB/GPU: 9.1ms



(l) TRD<sub>7×7</sub><sup>5</sup>, **37.64dB**/GPU: 20.3ms



(m) Noisy, 20.17dB



(n) BM3D, 33.24dB



(o) CSF<sub>7×7</sub><sup>5</sup>, 32.93dB



(p) WNNM, **33.77dB**



(q) TRD<sub>5×5</sub><sup>5</sup>, 32.91dB



(r) TRD<sub>7×7</sub><sup>5</sup>, 33.34dB

Figure 5. Denoising results on three test images ( $\sigma = 25$ ) by different methods (compared with BM3D [5], WNNM [7] and CSF model [12]), together with the corresponding computation time either on CPU or GPU. Note that for the last image, which contains many repeated local patterns, *e.g.*, the T-shirt region, the nonlocal methods (BM3D and WNNM) generally should work better than the local methods (CSF model and our TRD model), because the nonlocal models explicitly exploit nonlocal self-similarity across the image. Even though the nonlocal methods can benefit from these repeated local patterns, our trained TRD<sub>7×7</sub><sup>5</sup> still show strongly competitive performance. **Best viewed magnified on screen. Note the differences in the highlighted region.**



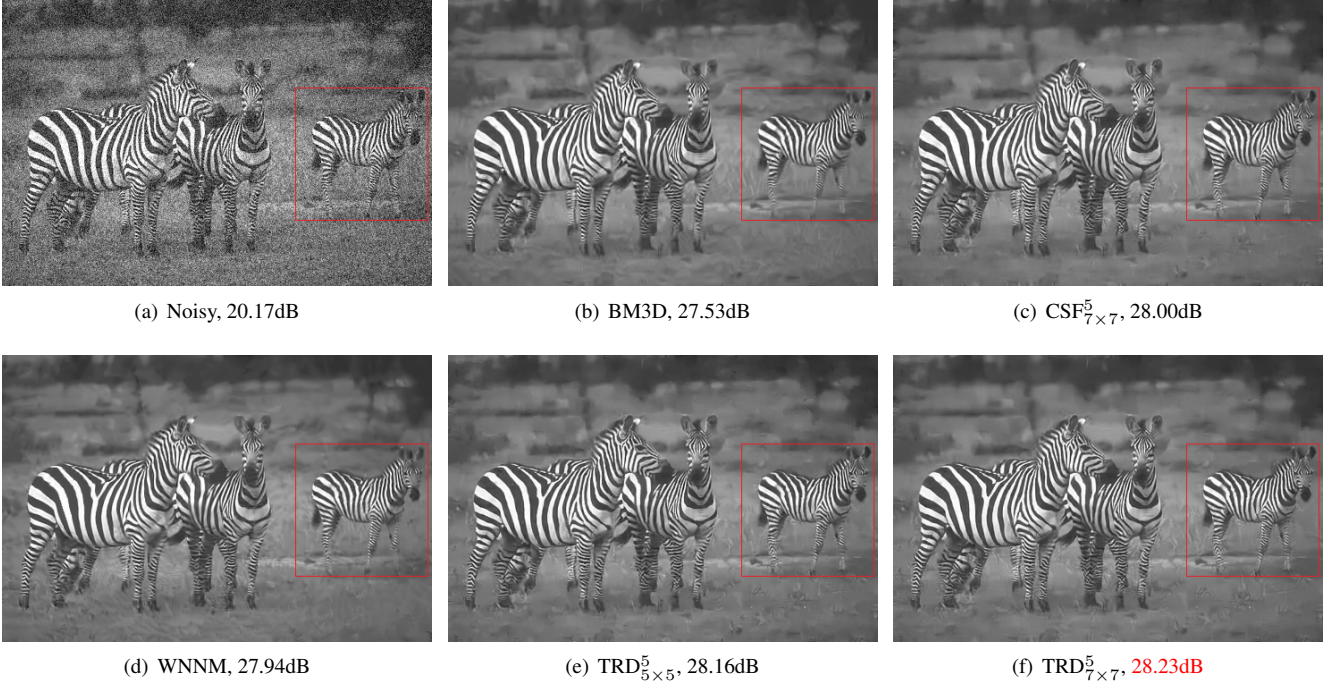


Figure 6. Another example noise level  $\sigma = 25$ . Note the differences in the highlighted region.

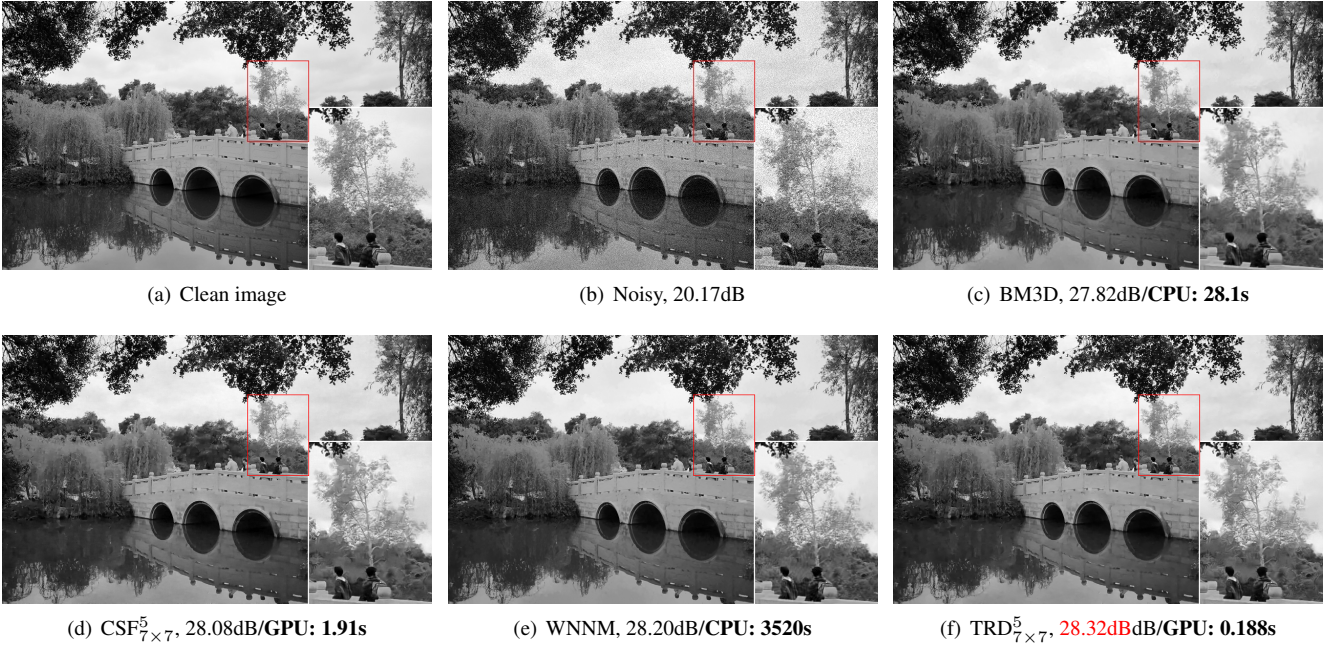


Figure 7. Denoising example on a high resolution “Chinese bridge” image of size  $1050 \times 1680$  ( $\sim 1.68$  mega-pixels) for noise level  $\sigma = 25$ . Compared with BM3D [5], WNNM [7] and CSF model [12], together with the corresponding runtime. Our TRD $_{7 \times 7}^5$  model achieves the highest PSNR value, and it better preserves tiny image structures, *e.g.*, the tree branches in the highlighted region. **(Best viewed magnified on screen.)** Moreover, our model offers remarkably preferable runtime performance based on GPU implementation.



Fig-1 Clean image



Fig-2 Clean image



Fig-3 Clean image



Fig-4 Clean image



Fig-5 Lossy image (30.02)



Fig-6 Lossy image (27.59)



Fig-7 Lossy image (24.24)



Fig-8 Lossy image (28.56)



Fig-9 TGV[2] (30.44)



Fig-10 TGV[2] (28.31)



Fig-11 TGV[2] (25.12)



Fig-12 TGV[2] (29.34)



Fig-13 Dic. SR[3] (30.50)



Fig-14 Dic. SR[3] (28.20)



Fig-15 Dic. SR[3] (25.11)



Fig-16 Dic. SR[3] (29.29)



Fig-17 SADCT[6] (30.69)



Fig-18 SADCT[6] (29.63)



Fig-19 SADCT[6] (25.54)



Fig-20 SADCT[6] (29.53)



Fig-21 RTF[9] (30.93)



Fig-22 RTF[9] (29.16)



Fig-23 RTF[9] (26.37)



Fig-24 RTF[9] (29.94)



Fig-25  $\text{TRD}_{7 \times 7}^4$  (31.04)



Fig-26  $\text{TRD}_{7 \times 7}^4$  (29.47)



Fig-27  $\text{TRD}_{7 \times 7}^4$  (27.05)



Fig-28  $\text{TRD}_{7 \times 7}^4$  (30.17)

Figure 8. Image deblocking for images compressed by JPEG encoder with the quality  $q = 10$ . **Note the differences in the sky.**